1993A&A...279..577P

Astron. Astrophys. 279, 577–588 (1993)

ASTRONOMY AND ASTROPHYSICS

The influence of ice-coated grains on protostellar spectra

Th. Preibisch[1], **V. Ossenkopf** [2], **H.W. Yorke**[1] **and Th. Henning** [2]

[1] Institut für Astronomie und Astrophysik der Universität Würzburg, Am Hubland, D-97074 Würzburg, Germany
Internet: preib@astro.uni-wuerzburg.dbp.de, yorke@astro.uni-wuerzburg.dbp.de
[2] Max-Planck-Gesellschaft, AG "Staub in Sternentstehungsgebieten", Schillergäßchen 2-3, D-07745 Jena, Germany

Received November 24, 1992; accepted June 26, 1993

Abstract. Information about protostellar sources obtained by fit calculations contain a number of uncertainties due to our poor knowledge of the properties of dust grains in dense clouds. From the results of recent observational and theoretical studies of dust in dense regions we construct a new dust model that consists of amorphous carbon grains and ice-coated silicate grains.

The model is based on new refractive indices of amorphous carbon and ice-coated silicate grains. Our model of the "dirty ice" assumes a mixture of H_2O and NH_3 ice with inclusions of amorphous carbon. The optical constants are calculated using effective-medium theory. We determine the opacities of core-mantle-particles with varying mantle thickness and pollution by spherical Mie calculations and investigate the effects on the spectrum of a embedded source.

The different models for the core-mantle-particles are used to fit the observed spectra of two protostellar sources and to determine the envelopes masses of these objects. We find considerable differences in the masses obtained from different dust models.

Key words: interstellar medium: dust – stars: circumstellar matter – stars: formation of – radiation transfer

1. Introduction

During the early phases of their evolution young stellar objects are embedded in a dense envelope of gas and dust which absorbs the stellar visible and NIR radiation and reradiates at FIR wavelengths. This allows no direct observation of the central object itself and one is forced to model the observed spectra with radiation transfer calculations in the dusty envelope. The resulting spectra and therefore the information one gets from the fit depend both on the optical properties of the dust grains and the envelope's structure. Unfortunately, the dust properties in dense clouds are only poorly known. Therefore, there are some uncertainties in such fit calculations and the results have to be treated with some caution (see e.g. Butner et al. 1991).

In the dense star forming regions of molecular clouds the formation of mantles of "ice" by the accretion of gas molecules onto cool grains is theoretically expected and observationally established (Draine 1985a). These coated grains can considerably influence the opacity of the dust.

It is the aim of this paper to estimate possible errors that arise from the uncertanties in the dust properties produced by ice coatings. Several models for coated grains are constructed and frequency dependent exact radiation transport calculations are performed in spherical symmetry. We calculate spectra of protostellar sources embedded in dusty envelopes with different dust models and compared the results. Fit calculations of the observed spectra of protostellar sources are performed with the different dust models used to determine the envelope mass of selected sources.

We will refer to the 0.8 – 5 μm region as the near-infrared (NIR), to the 5 – 30 μm region as the mid-infrared (MIR), to the 30 – 300 μm region as the far-infrared (FIR) and to the 300 – 3000 μm region, although not strictly correct, as the submm-region.

Send offprint requests to: H.W. Yorke

2. Dust models

2.1. Construction of dust models

Using Mie theory, it is possible to determine the frequency dependent cross-sections for scattering and absorption of spherical homogeneous or homogeneously coated particles when the complex refractive indices of the involved materials are known as function of wavelength (Bohren & Huffman 1983). The quantities of interest in radiation transfer are the absorption and scattering cross sections of the grains $C_\nu^{\rm abs}$ and $C_\nu^{\rm sca}$. The extinction cross section, we will consider in the following, is defined as the sum of these: $C_\nu^{\rm ext} = C_\nu^{\rm abs} + C_\nu^{\rm sca}$. Often the extinction efficiency $Q_\nu^{\rm ext} = C_\nu^{\rm ext}/\pi a^2$ is used instead of the extinction cross section. Here a is the radius of the grain.

The extinction coefficient $\sigma_\nu^{\rm ext}$ is given by $\sigma_\nu^{\rm ext} = n\,C_\nu^{\rm ext}$, where n is the number density of grains. In the dusty envelope

© European Southern Observatory • Provided by the NASA Astrophysics Data System

1993A&A...279..577P

of a protostar the total extinction of the dust is many orders of magnitude higher than that of the gas (Pollack et al. 1985). Therefore the contribution of the gas to the coefficients can be neglected.

Since the grains exhibit a size distribution, one has to integrate over all grain radii a for a total cross section. Taking into account that there are several sorts i of grains (e.g. carbon grains and silicates) one gets

$$\sigma_{\nu,i} = \int n_i(a)\, C_{\nu,i}(a)\, \mathrm{d}a \qquad (1)$$

where $n_i(a)$ characterizes the size distribution of grain type i. The total coefficient can be written as the sum over all dust components: $\sigma_\nu = \sum_i \sigma_{\nu,i}$.

Since the number density of grains is about proportional to the mass density of the interstellar matter, a frequently used quantity for the strength of the interaction between the dust and the radiation field is the *gram opacity* of the dust κ_ν. It is defined as

$$\kappa_\nu := \frac{\sigma_\nu}{\rho} = \sum_i \frac{1}{\rho} \int n_i(a)\, C_{\nu,i}(a)\, \mathrm{d}a\,, \qquad (2)$$

where ρ is the total density of gas and dust.

2.2. *Differences between dust in diffuse clouds and in dense regions*

Many dust models in use are based on the particle model of Draine & Lee (1984) consisting of two kinds of materials, graphite and "astronomical silicate". Mathis et al. (1977) proposed a size distribution of the grains in the form $n(a) \propto a^{-3.5}$ for $a_{\min} \leq a \leq a_{\max}$. With $a_{\min} = 5\,\mathrm{nm}$ and $a_{\max} = 250\,\mathrm{nm}$ Draine & Lee (1984) were able to fit the observed extinction curve of the diffuse interstellar medium quite well.

For a model of dust in dense molecular clouds, the sites of star formation, one has to take into account a number of differences to the dust in diffuse clouds. First, there are observational results that the grains in dense clouds are considerably larger (Draine 1985a; Tielens 1989; Chen & Graham 1993) and perhaps have a fluffy structure (Ossenkopf 1993). Second, many objects embedded in dense clouds show a prominent absorption feature at 3.07 μm, that is generaly attributed to ice coatings on the surface of the grains (Tielens 1989). Third it is found that the 220 nm band indicating graphite grains, is much weaker in dense regions or even absent (Sorrell 1990a).

Therefore, the Draine & Lee dust model, that applies to dust in diffuse clouds, cannot be used without modification when treating dense regions.

2.3. *Basic presumptions for a dust model for star forming regions*

Our dust model for dense regions consists of three components: Small amorphous carbon grains, large silicate grains and a mantle of "dirty ice" at the surface of the silicate grains when their temperature is low enough. The individual components will be decribed here in detail.

2.3.1. Amorphous carbon (aC)

Up to the beginning of the 1980s cosmic carbon grains were generally believed to exist as graphite. However, similar to the case for carbon grains in the shells of late-type stars (Czyzak & Santiago 1973; Martin & Rogers 1987) there is growing evidence that carbon grains in molecular clouds and cold parts of protostellar disks must be highly amorphous (sometimes also called glassy or vitrious). This follows from the investigation of the structural chemistry of carbon grains under cosmic conditions (Sorrell 1990a) and from radiative transfer calculations in protostellar disks. The observed FIR fluxes can be explained by a dust material with an emissivity in the FIR proportional to λ^{-1} instead of the λ^{-2} expected from graphite for $\lambda \gtrsim 30$ μm. Amorphous carbon is a material which may exhibit such a behaviour.

There are three quantities characterizing the structure of disordered carbon grains.

(i) There is short range order in the solid material determined by the hybridization state of the carbon atoms sp^2 (graphite-like) or sp^3 (diamond-like) bonding. Graphite-like bondings are associated with the 220-nm plasmon band and a low optical gap expressed by an high absorptivity at UV and visible wavelengths.

(ii) The second characteristic quantity is the amount of hydrogen bond into the carbon grains. This hydrogen directly influences the short range structure and produces the characteristic resonances of C-H vibrations. One prominent feature appears at 3.3 μm for aromatic C-H vibrations and at 3.4 μm for vibrations in aliphatic structures.

(iii) The third characteristic quantity is the long range order in the grains. In the case of the "aromatic" grains it gives the correlation between neighbouring graphitic layers. This parameter distinguishes between crystalline or polycrystalline graphite and so-called glassy carbon with a lack of this long range order. In the aliphatic case it distinguishes between a regular diamond lattice and a glass-like network structure often called amorphous carbon. All four structures are observed under cosmic conditions.

The relation between cosmic conditions and structural changes in the carbon grains was investigated by Sorrell (1990 a,b). He found that the ratio between the number of aromatic and aliphatic bondings in the grains depends on the UV radiation density and the hydrogen gas density in the grain environment. The UV radiation increases the number of graphitic bondings and the hydrogen adsorption changes graphitic into diamond-like bondings. Moreover, the splitting up of single aromatic bondings by hydrogen significantly disturbes the long range order of the lattice, destroying the correlation between remaining graphitic planes. Heated grains in the ISM tend to form aromatic structures and tend to crystallize while cooler grains in denser regions stay amorphous and prefer aliphatic bondings.

The main parameters in the opacity spectrum of amorphous carbon are the power law exponent in the infrared region and the absolute value of the absorption coefficient. It can be shown theoretically (Kittel 1963) that grains dominated by two-

© European Southern Observatory • Provided by the NASA Astrophysics Data System

1993A&A...279..577P

Table 1. Complex refractive indices of our models for aC and dirty ice with 10 Vol-% aC-pollution (see Sect. 2.3.1 and 2.3.3)

	aC		dirty ice			aC		dirty ice			aC		dirty ice	
λ [μm]	n	k	n	k	λ [μm]	n	k	n	k	λ [μm]	n	k	n	k
0.105	1.415	0.796	1.346	0.081	7.036	3.200	0.947	1.483	0.083	48.68	4.558	1.739	1.804	0.545
0.207	1.617	0.512	1.358	0.048	7.451	3.241	0.989	1.479	0.079	51.51	4.623	1.763	1.887	0.465
0.410	1.879	0.774	1.388	0.065	7.887	3.291	1.028	1.464	0.076	54.52	4.667	1.785	1.903	0.369
0.810	2.318	0.773	1.420	0.053	8.349	3.355	1.060	1.435	0.075	57.72	4.701	1.824	1.867	0.340
1.077	2.445	0.766	1.427	0.050	8.837	3.428	1.070	1.437	0.122	61.10	4.744	1.877	1.865	0.359
1.207	2.501	0.761	1.429	0.048	9.350	3.485	1.056	1.462	0.102	64.67	4.797	1.928	1.900	0.372
1.515	2.594	0.759	1.430	0.046	9.903	3.523	1.049	1.407	0.093	68.46	4.848	1.970	1.944	0.362
1.698	2.641	0.773	1.429	0.046	10.48	3.550	1.036	1.362	0.143	72.46	4.891	2.031	1.980	0.334
1.902	2.695	0.784	1.426	0.045	11.74	3.614	1.064	1.386	0.319	76.72	4.953	2.080	2.000	0.308
2.014	2.725	0.788	1.424	0.045	12.43	3.638	1.070	1.466	0.369	81.19	4.990	2.136	2.019	0.281
2.256	2.785	0.799	1.414	0.044	13.16	3.669	1.086	1.556	0.386	85.98	5.041	2.211	2.039	0.253
2.388	2.818	0.801	1.405	0.043	13.93	3.706	1.096	1.635	0.361	90.96	5.095	2.280	2.057	0.222
2.528	2.849	0.800	1.393	0.042	14.74	3.733	1.100	1.692	0.318	96.33	5.144	2.365	2.059	0.180
2.676	2.879	0.800	1.357	0.041	15.60	3.751	1.118	1.725	0.269	102.0	5.213	2.461	2.055	0.143
2.832	2.909	0.798	1.243	0.094	16.52	3.785	1.145	1.734	0.215	107.9	5.292	2.549	2.035	0.119
2.998	2.935	0.796	1.364	0.364	17.48	3.815	1.150	1.730	0.187	114.3	5.369	2.642	2.018	0.106
3.174	2.962	0.798	1.634	0.243	18.51	3.835	1.190	1.725	0.165	121.0	5.459	2.745	2.004	0.100
3.360	2.997	0.796	1.566	0.097	19.59	3.877	1.196	1.729	0.139	135.5	5.661	2.926	1.992	0.095
3.556	3.020	0.776	1.544	0.086	21.95	3.938	1.292	1.706	0.085	143.4	5.755	3.037	1.990	0.094
3.764	3.025	0.778	1.528	0.063	23.24	3.994	1.298	1.684	0.072	160.7	6.026	3.254	1.990	0.089
3.984	3.045	0.786	1.509	0.056	24.59	4.016	1.328	1.659	0.065	170.1	6.183	3.354	1.990	0.087
4.217	3.065	0.792	1.495	0.058	26.04	4.067	1.363	1.635	0.060	190.6	6.521	3.489	1.990	0.081
4.464	3.087	0.798	1.492	0.064	27.56	4.108	1.381	1.608	0.056	213.5	6.752	3.607	1.991	0.076
4.727	3.109	0.803	1.495	0.059	29.17	4.144	1.423	1.579	0.062	239.3	7.103	3.804	1.994	0.070
5.003	3.131	0.804	1.485	0.054	30.88	4.201	1.444	1.545	0.084	268.1	7.530	3.917	1.996	0.063
5.296	3.147	0.803	1.474	0.053	34.59	4.299	1.493	1.479	0.156	300.4	7.877	3.887	1.996	0.057
5.605	3.150	0.804	1.454	0.061	36.63	4.320	1.529	1.450	0.220	400.0	8.732	4.246	2.001	0.046
5.932	3.143	0.823	1.456	0.097	41.04	4.403	1.586	1.446	0.379	500.0	9.730	4.418	2.005	0.037
6.281	3.149	0.865	1.481	0.100	43.44	4.438	1.636	1.543	0.497	600.0	10.629	4.103	2.006	0.030
6.648	3.172	0.905	1.487	0.088	45.97	4.489	1.693	1.658	0.590	800.0	11.438	3.800	2.007	0.024

dimensional structures exhibit an absorption behaviour like λ^{-1}, while grains built up of three-dimensional sub-units behave like λ^{-2} at long wavelengths. Thus there are two ways to produce a λ^{-2}-behaviour in disordered carbon grains. One is the formation of an sp^3-dominated spatial network guaranteeing the 3-D structure and the other is the formation of microislands of compact graphite with a tight correlation between the graphite layers within the islands. A λ^{-1}-behaviour can only be produced if relatively large graphitic planes exist, which are hardly correlated to each other. The absolute value of the absorption coefficient in the visible and NIR wavelength region is determined by the optical gap energy. An increasing number of aromatic bonds in the material produces an decreasing optical gap and an increasing absorptivity in this wavelength range.

There are numerous laboratory measurements on optical properties of amorphous carbon. The resulting absorption coefficients differ sometimes by orders of magnitudes. Unfortunately, the structure of all samples is not known in terms of the critical parameters described above. Hence, we had often to take the reverse way of deriving conclusions on the structure of the samples from knowledge of the measured optical behaviour and the description of the production technique.

We found e.g. that the optical constants for amorphous carbon given by Edoh (1983) which are often used in astronomical simulations can be well reproduced by an uncorrelated, polycrystalline aggregate of small graphite islands all containing some well correlated graphitic planes. Looking at the production method it seems probable that the original material was not completely vapourized or that the cooling rate was not fast enough to prevent the reformation of such graphitic islands. The material is only weakly amorphous.

From the published samples we selected the "BE" material measured by Bussoletti et al. (1987, between 0.1 and 300 μm) and Blanco et al. (1991, between 40 and 700 μm) to be the best representative for the amorphous carbon in cold dense regions. The measured visible and NIR absorption indicates an intermediate sp^2/sp^3 ratio in the grains. The low wavelength exponent of the FIR decay of the absorption ($\beta \approx 1.2$ for spheres) gives evidence for the existence of graphitic planes only weakly correlated to each other in the grains. The production procedure

© European Southern Observatory • Provided by the NASA Astrophysics Data System

1993A&A...279..577P

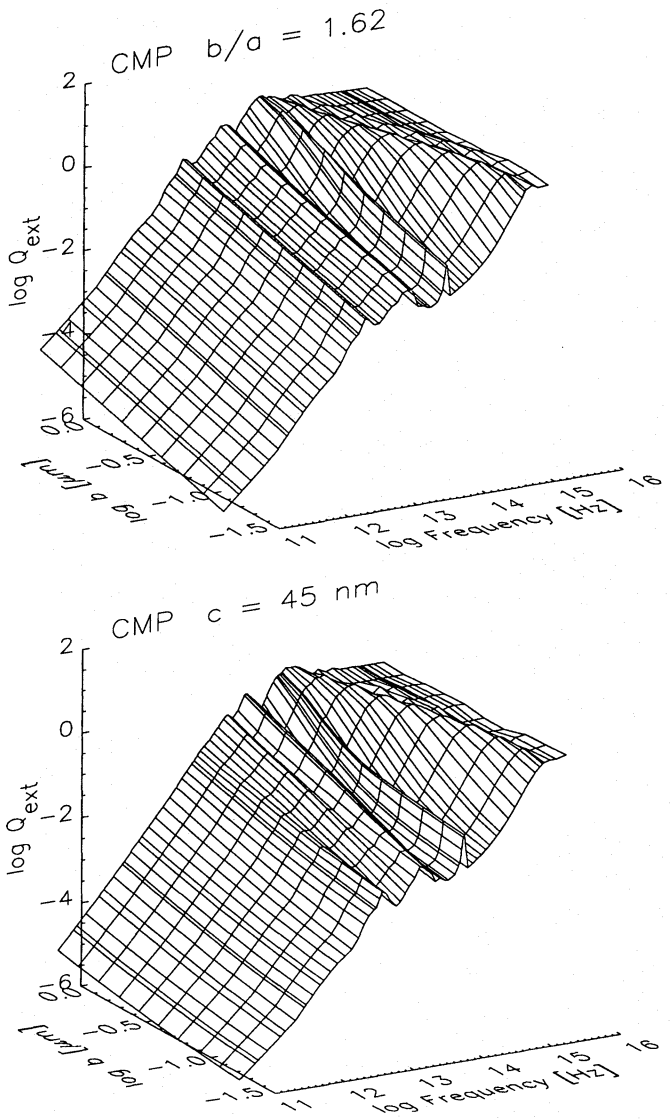

Fig. 1. Extinction efficiency of the CMP with b/a = 1.62 and with c = 45 nm

(burning of benzene in air) comprises the production of polluted carbon with remaining or newly produced C-H and C-O bondings in the sample. This is just what one expects for the cold regions in molecular clouds and the outer parts of protostellar disks.

Bussoletti et al. (1987) and Blanco et al. (1991) published only absorption coefficients for their grains. Rouleau & Martin (1991) derived optical constants from the Bussoletti data using a technique taking shape and clustering effects into account. Using the same technique we extend the available optical constants on the basis of the more recent measurements of Blanco et al. (1991) up to 800 μm. The complex refractive indices used are given in Table 1. Sorrell (1990a) showed that aC grains with radii $a \gtrsim 10-50$ nm will be rapidly destroyed by hydrogenation and chemical sputtering in dense clouds. Therefore we chose a power law size distribution in the form

$$n(a) \propto a^{-3.5} \quad \text{for} \quad 7\,\text{nm} \leq a \leq 30\,\text{nm}\,. \tag{3}$$

This means that all grains are well within the Rayleigh limit (condition $2\pi a \ll \lambda$) for wavelengths above 1 μm. In this limit, the size of the grains and so the exact boundary values of the distribution have no influence on the gram opacity of the dust κ because $C_\nu(a)$ is proportional to the dust mass.

Spectra of embedded IR sources typically peak at $\lambda \approx 100\,\mu$m and fluxes below 1 μm depend sensitively on the density distribution within the envelope as well as the scattering properties of the grains, so that the part of the spectrum below 1 μm cannot easily be used for obtaining information on the protostellar object. Hence, for the "interesting" part of the spectrum the exact size of the aC grains is unimportant.

The opacity spectrum of the aC grains is shown in Fig. 3. The opacity values were extrapolated to mm-wavelengths using the same slope as between 500 and 800 μm. In all dust models we use 60 % of the carbon atoms available from the cosmic abundances for the total amount of aC in the dust – corresponding to 2.2×10^{-4} C atoms in aC per gaseous H atom using the cosmic abundances of Lang (1974).

2.3.2. Silicate

The second component of our dust model is silicate grains. The existence of silicate grains is widely established, although the exact chemical composition is not clear (see e.g. Ossenkopf, Henning & Mathis 1992). We use the optical data for the "astronomical silicate" of Draine & Lee (1984), tabulated in Draine (1985b).

We assume the same power law size distribution as for aC grains, but change the cut-offs. To take the observational results on the presence of large grains in dense regions into account, we choose $a_{\min}$ = 40 nm and $a_{\max}$ = 1 μm. These radii are not thought to be the exact boundaries of the size distribution; they simply match the order of the grain sizes in dense molecular clouds. For example, Pendleton et al. (1989) found grain sizes $a \approx 0.5\,\mu$m in their study of Orion molecular clouds, and Hyland & Robinson (1991) determined grain sizes $a \approx 1\,\mu$m from the spectum of AG Carinae. For wavelengths above 10 μm the limits play no role since the grains are also in the Rayleigh limit. From the heavy depletion of the silicon abundance in dark clouds (e.g. Morton 1974), we assume that the silicate grains contain all Si atoms available from the cosmic abundances. So we have 3.1×10^{-5} Si atoms per H atom in form of silicate. The opacity of the pure silicate grains is shown in Fig. 3.

2.3.3. Dirty ice mantles

The third component are the coatings of "dirty ice" around the silicate grains, if their temperature is below 125 K. We will denote these coated particles as *core-mantle-particles* (CMP). Since even in dense cores of molecular clouds the density is too

© European Southern Observatory • Provided by the NASA Astrophysics Data System

1993A&A...279..577P

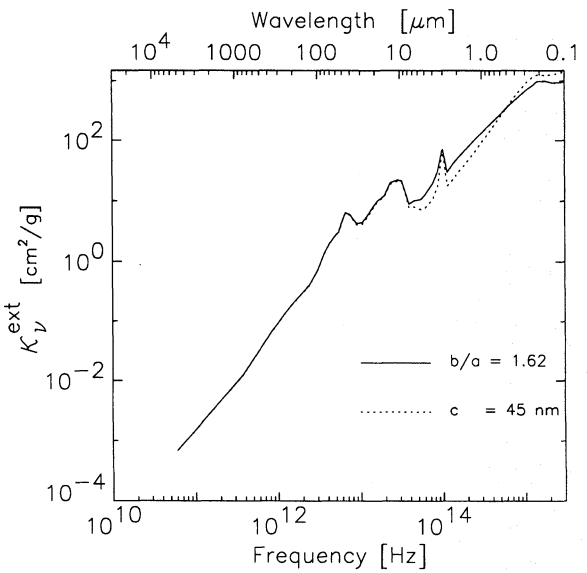

Fig. 2. Opacity spectrum for the models from Fig. 1 but integrated over the full size distribution

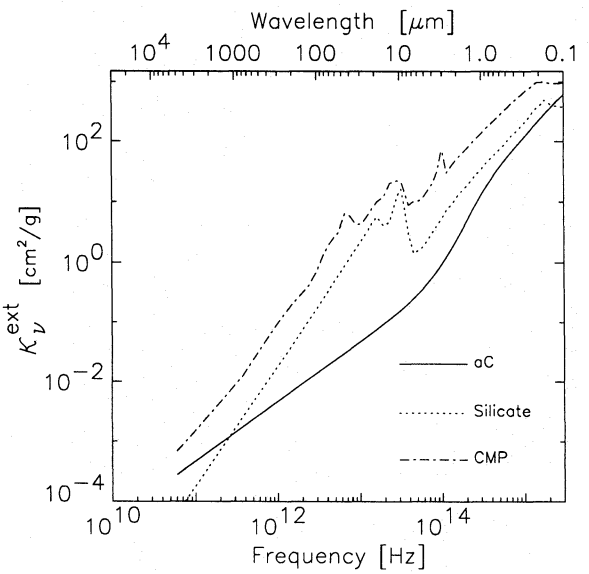

Fig. 3. Contribution of the dust components to the opacity

low to allow condensation of pure gaseous substances, condensation can only take place at the surface of cold grains (Seki & Hasegawa 1983). The coatings are thought to be formed when gas phase molecules are accreted on a grain surface and reactions between different molecules take place (Tielens & Hagen 1982).

The main constituents of this "ice" should be H_2O, NH_3, CO and some other simple molecules. The exact composition is very uncertain and reflects the physical conditions and history of the individual cloud. The prominent absorption feature at 3.1 μm generally attributed to O–H streching vibrations of water ice (Emerson 1988) is observed in many embedded objects. Hagen et al. (1983) found that a mixture of H_2O and NH_3 ice with a volume ratio of 3:1 fits the shape of the 3.1 μm feature toward the Becklin-Neugebauer object very well.

During the formation of the mantles it is possible that other grains, especially the numerous and small aC grains will stick to the surface and be included in the mantles. Moreover carbonaceous pollutions can be formed by chemical reactions of CO and organic molecules induced by cosmic rays. This pollution of the ice mantles has considerable influence on the optical properties of the CMP, as will be shown in the following section.

The optical constants of our dirty ice model shall be valid for a mixture of H_2O- and NH_3-ice with a volume ratio of 3:1, that is polluted with amorphous carbon. The refractive index of the pure ice was constructed from three data sources: In the range of 2.5 – 15 μm the values of Mukai & Krätschmer (1986) for the assumed ice-mixture were used. The continuation to longer wavelengths was obtained from the values of Leger et al. (1983) for pure H_2O-ice. Here, the strength of the 43 μm band of the ice was reduced in proportion to the ratio of the 12 μm bands as given by Leger et al. (1983) for pure H_2O-ice and by Mukai & Krätschmer (1986) for their ice-mixture. For shorter wavelengths (1 μm $< \lambda <$ 2.5 μm) a smooth transition to the values given by Lee & Draine (1985) was introduced without adding any further absorption features. The Kramers-Kronig consistency of the combined set was reproduced by small changes in the real refractive index. From the refractive indices of ice and amorpous carbon and the volume-portion of the carbon pollution the refractive index of the dirty ice was calculated by means of effective-medium theories (Ossenkopf 1991). The values for ice with 10 Vol-% pollution are also given in Table 1.

We will not assume ice coatings on the aC grains since they are so small that temperature spikes produced by single photon absorption or cosmic rays can prevent the formation of ice mantles (Yorke 1985).

We assume that all mantles will sublimate if the temperature of the CMP rises above 125 K. From every CMP there remains one silicate grain and several aC grains, depending on the amount of the pollution of the ice. In the radiative transfer calculations this is simulated by a temperature limit at which the CMP particles are retransformed to bare silicate and aC grains so that the total number of aC atoms is conserved.

In this paper we will demonstrate the effects of these coatings on calculated spectra of protostellar objects. Several different possibilities for the ice mantles are investigated.

The opacity of the CMP can be calculated as a function of the silicate core radius a and the outer mantle radius of the whole particle b by Mie theory. While the core radii a are simply given by the size distribution of the silicate grains, there are several possibilities for the choice of the coating thickness.

The first is to assume the mantle thickness to be simply proportional to the core radius, so that $b/a = const.$ In the literature a wide range of values for the relative mantle thickness can be found: Leung (1975) e.g. uses very thick coatings with $b/a = 3$, while Ossenkopf (1991) assumes $b/a = 1.145$. Three possibilities will be considered here: $b/a = 1.145$, $b/a = 1.62$

© European Southern Observatory • Provided by the NASA Astrophysics Data System

1993A&A...279..577P

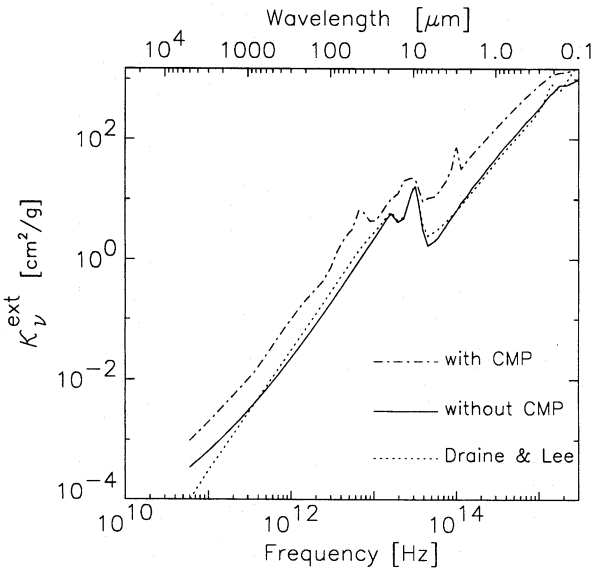

Fig. 4. Comparison of the Draine & Lee model with our dust model from Fig. 3 in the case of coated and uncoated silicates

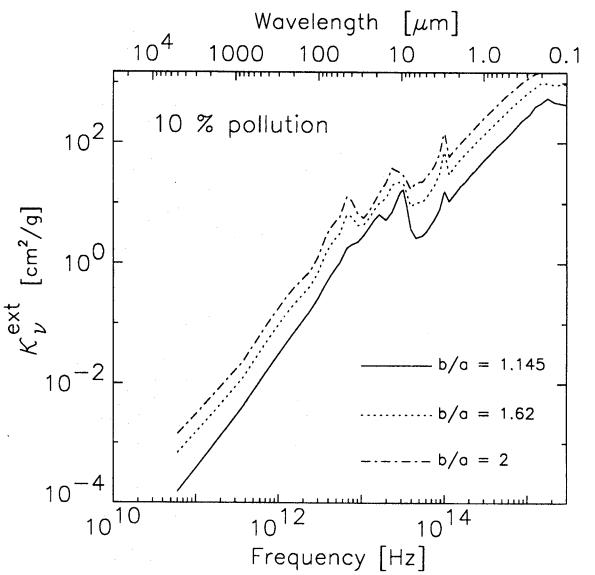

Fig. 5. CMP opacity for b/a = 1.145, b/a = 1.62 and b/a = 2

and $b/a = 2$ according to ice to silicate volume ratios of 0.50, 3.25 and 7.00 respectively.

A second possibility is to assume that the coating thickness c is independent of the core radius, $c = const.$ Tielens (1989) used c = 3 nm, whereas Draine (1985a) found $c \approx 16$ nm. Here we examine three models with mantle thicknesses of c = 3 nm, c = 12 nm and c = 45 nm. The total ice to silicate volume for the assumed size distibution is then 0.11, 0.50 and 3.25 respectively.

Another free parameter is the pollution of the ice. We calculated models with pollutions of 5, 10, and 20 Vol-% aC.

All dust models contain the same number of carbon atoms but the distribution of the carbon atoms between the pollution of the ice mantles and the free aC grains is very different. The percentage of the aC needed for the pollution of the ice mantles ranges from 0.008 % for c = 3 nm and 5 Vol-% pollution up to 98 % for b/a = 2 and 10 Vol-% pollution. A model with b/a = 2 and 20 Vol-% pollution is excluded since more than the available amount of carbon would be needed. The amount of oxygen and nitrogen in the ice mantles is always below the available numbers of atoms.

As examples for the optical properties of our CMP we show the extinction efficiency of two CMP models as a function of the frequency and the total radius of the CMP in Fig. 1. The upper part shows the model with coatings proportional to the core radius and b/a = 1.62 and the lower part the model with a fixed coating thickness of 45 nm each with a pollution of 10 Vol-% aC in the ice. Both models coincide for mean particle radii b of 117.6 nm.

Three prominent absorption features can be seen: The silicate feature at 9.7 μm and two ice features at 3.1 μm and 43 μm. One can well follow the decrease of the ice features relative to the silicate features with increasing grain size in the model with constant coating thickness. In the b/a =const. model the ratio remains constant up to grain sizes of about 1 μm. In both cases one sees the shift of the limit of the violation of the Rayleigh behaviour towards longer wavelengths with growing grain size.

In Fig. 2 the integrated opacity for the assumed size distributions of both models is shown. One sees that both models lead to nearly the same opacity behaviour above 10 μm because the total ice content is identical. The model with c = 45 nm shows a stronger 3.1 μm ice-feature, because here the numerous small grains have a larger mantle thickness than in the b/a = 1.62 model.

In Fig. 3 we show the opacities of the three dust components, aC, silicates and CMP. For the CMP model we used b/a = 1.62 and a pollution of 10 Vol-%. In this model 45.7 % of the aC is needed for the pollution of the mantles and the remaining 54.3 % is in form of free aC grains.

Figure 4 shows the sum opacity in comparison with the dust model of Draine & Lee. In the case of uncoated silicates our dust model differs significantly from the Draine & Lee model only at the largest wavelengths. That is due to the presence of aC instead of graphite in our model. If the silicates are coated, the total opacity is enhanced throughout the spectrum. This is both due to the addition of dust mass in the form of ice mantles and the higher absorptivity of the carbon grains when they are embedded in the ice mantles. The spectral slope of our opacity is noticeably lower at large wavelengths than that of the Draine & Lee model.

2.4. Variation of the CMP properties and resulting opacities

In this section we will compare the opacity of CMP models with different coating thickness and with different amounts of pollution. First, we assume a pollution of the ice with 10 Vol-% aC and compare CMP models with variable coating thickness and the values b/a = 1.145, b/a = 1.62 and b/a = 2.

© European Southern Observatory • Provided by the NASA Astrophysics Data System

1993A&A...279..577P

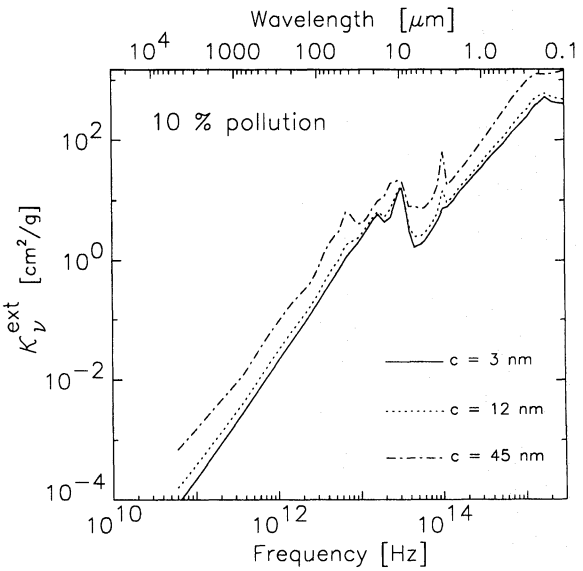

Fig. 6. CMP opacity for $c = 3$ nm, $c = 12$ nm and $c = 45$ nm

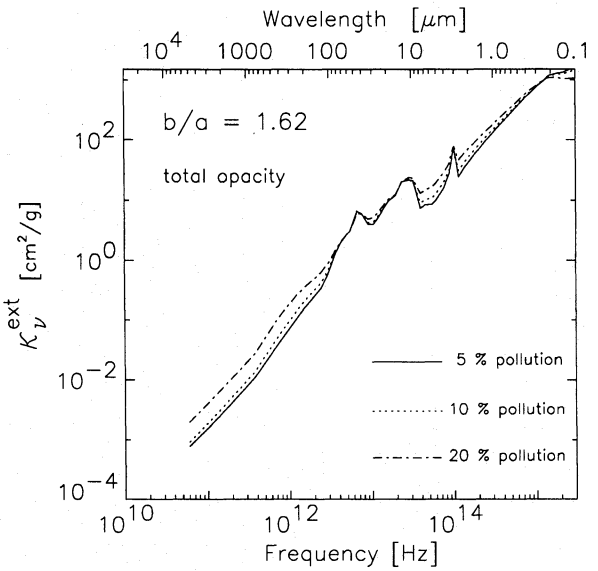

Fig. 7. Total (CMP + aC) opacity for $b/a = 1.62$ and aC pollutions of 20 Vol-%, 10 Vol-% and 5 Vol-%

In Fig. 5 we show the opacity of the CMP grains for these models. One can see that the prominence of the ice feature at 3.07 μm is only slightly enhanced with increasing coating thickness, while the ice feature at 42 μm grows much stronger. The silicate feature weakens at the same time, but another ice feature at 12 μm grows and together they produce a broad feature. The opacity grows over the whole spectral range.

In Fig. 6 the opacities of three models with constant coating thickness of $c = 3$ nm, $c = 12$ nm and $c = 45$ nm are compared. The 10 μm region shows similar changes as in the case of variable coating thickness. Here the 3.07 μm ice feature grows faster than the the 42 μm feature.

In order to investigate the influence of the pollution, we compare in Fig. 7 models with $b/a = 1.5$ and 20 Vol-%, 10 Vol-% and 5 Vol-% pollution. Here, we show the sum opacities of the CMP and the free aC grains to eliminate the effect of changing total carbon content. A smoothing of the ice features and the short wavelength side of the silicate feature with increasing pollution can be well followed. Whereas the peak values of the features remain constant, the FIR opacities are considerably enhanced with increasing pollution. Note that the grain size is equal and the total mass of dust is nearly equal for the three models. This means that the amorphous carbon absorbs more effectively in the ice mantles than as free grains.

The spectral indices of the CMP in the FIR vary between 1.96 for the $c = 3$ nm model with 5 Vol-% carbon pollution and 1.45 for the $c = 45$ nm model with 20 Vol-% pollution. The corresponding spectral indices for the sum of all dust components are 1.35 and 1.45, respectively. Thus the total spectral index is not very sensitive to the ice mantle structure.

In Fig. 8 we show the Rosseland and Planck means for the total opacities of the models with variable b/a and 10 Vol-% pollution. The edges in the curves are due to the sublimation of the ice mantles, the silicate and then the aC grains (see Sect. 3).

3. Radiation transfer calculations

A frequently used method to obtain information on protostellar objects is to fit the observed spectrum of the protostellar source with numerical radiative transfer calculations. It allows one to determine essential quantities, e.g. the mass of the dust envelope (see Zinnecker et al. 1992).

Here we want to investigate how uncertanties in the dust models influence the results of such calculations. First, we assume a defined model protostar and compare its spectra calculated with the different dust models. Then we use our dust models to fit the spectra of two protostellar sources and determine the mass of the envelopes.

The radiation transfer calculations were carried out with a modified version of the code (without hydrodynamics) described in Yorke (1980a,b). This program yields an exact solution of the frequency dependent radiation transfer problem in extended spherical envelopes simultaneous with a self-consistent determination of the dust temperatures. One has to specify the luminosity and the effective temperature of the central source, the density distribution including the outer radius of the shell, the total mass of the envelope and the temperature and frequency dependent absorption and scattering gram opacity of the dust. "Observables" such as the overall spectrum and the flux distribution (limb-darkening) at each frequency can then be determined.

Because of the large variation of the scales, we assume logarithmically equidistant distribution of 120 radial grid points. The temperature dependence of the opacity is given by the sublimation temperatures of the grains. We used the values $T_{\rm sub}^{\rm aC} = 2000$ K, $T_{\rm sub}^{\rm Sil} = 1500$ K and $T_{\rm sub}^{\rm CMP} = 125$ K. The destruction of the grains through sublimation is simulated by setting the number density of the grains to zero, if the temperature of a particular grain component calculated simultaneously with the

© European Southern Observatory • Provided by the NASA Astrophysics Data System

1993A&A...279..577P

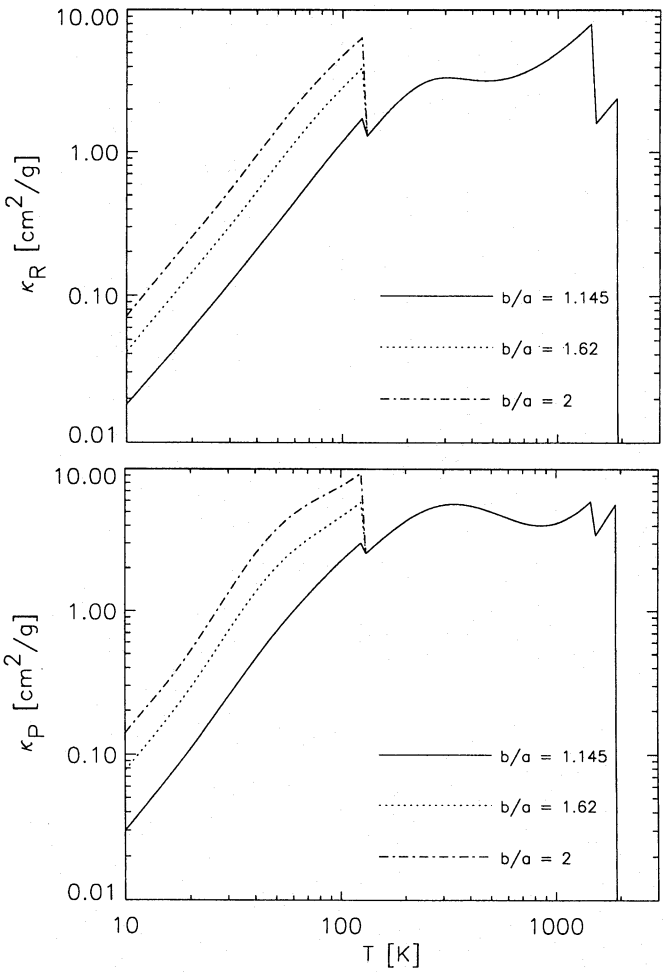

Fig. 8. Rosseland mean (κ_R) and Planck mean (κ_P) of the total opacities of the dust models with variable b/a and 10 Vol-% pollution

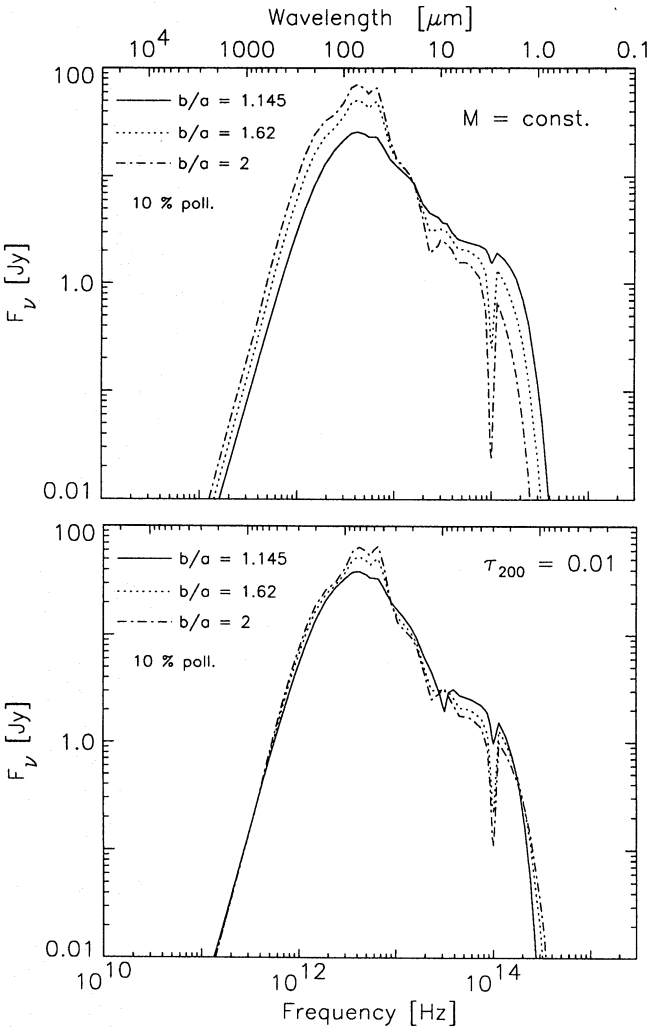

Fig. 9. Spectra of the model envelope calculated with the different CMP models: $b/a = 1.145$, $b/a = 1.62$ and $b/a = 2$ each with 10 Vol-% pollution

radiation field is above the sublimation temperature. So the inner boundary radius of the dust shell is given by the smallest sublimation radius of the dust components. When the ice mantles are destroyed above 125 K, silicate grains are added and the number density of the aC grains is enhanced so that the total amount of aC remains constant. The real values of the sublimation temperatures are uncertain, but Preibisch (1992) could show that a variation of the values up to 50 % does not lead to detectable changes in the calculated spectra for the class of objects considered here.

The density of the envelope can be characterized by the total optical depth at a certain wavelength. Here we choose the value at 200 μm, τ_{200}.

The applicability of the spherically symmetric code is justified for highly embedded sources because the accretion disks around protostars expected from theoretical calculations (see Boss 1987; Yorke et al. 1993) are generally restricted to radii of $\approx$ 100 AU for low mass protostars, whereas a typical cloud core has a radius of several 1000 AU. The outer envelope (R > 100 AU) is expected to be approximately spherical (Shu et al. 1987) and, if the outer envelope is dense enough, what is the case for the deeply embedded objects considered here, most of the information on the inner structure is lost (Yorke & Shustov 1981). A flattened structure in the center would affect the spectrum mainly in the optical and NIR part.

The dependence of the calculated flux spectrum on the input parameters of the model is given by the following results:

- The shape of the spectrum is very sensitive to changes of the mass of the envelope and L/R^2 where L is the luminosity of the protostar and R the outer radius of the envelope.
- The overall spectrum is nearly independent of the effective temperature of the protostar over a large range, since nearly all of the radiation of the protostar is absorbed in the envelope.
- The NIR region of the spectrum depends very strongly on the density distribution of the envelope and on the scattering properties of the grains. It could also be affected by a flattened structure in the center of the cloud and the viewing angle.

© European Southern Observatory • Provided by the NASA Astrophysics Data System

1993A&A...279..577P

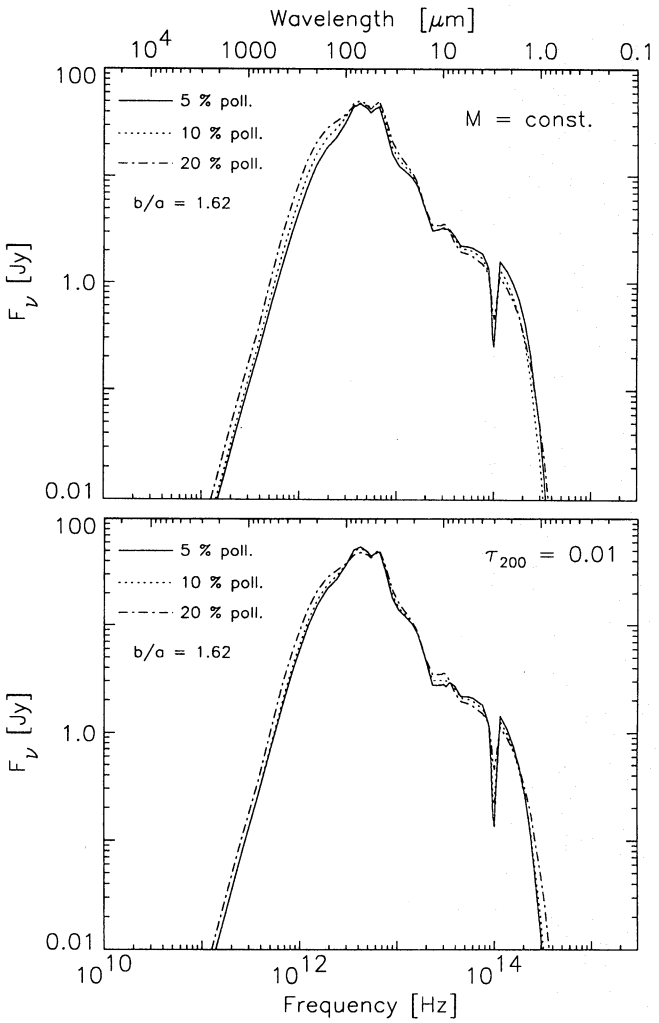

Fig. 10. Spectra calculated with the CMP models with $b/a = 1.62$ and pollutions of 5 Vol-%, 10 Vol-% and 20 Vol-%

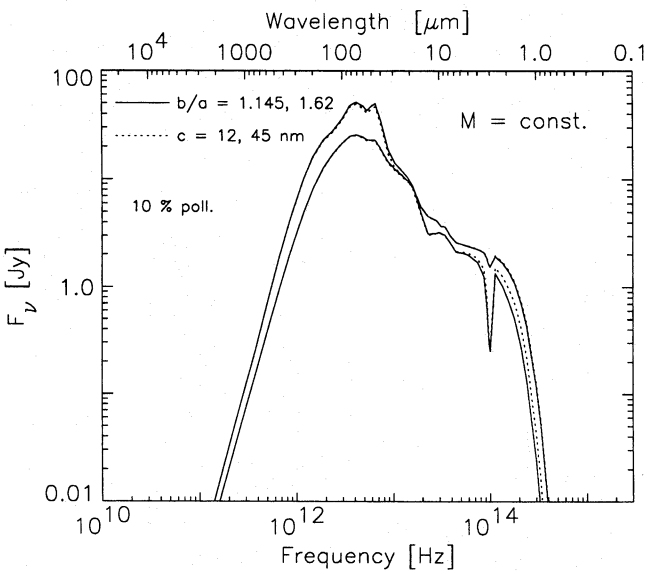

Fig. 11. Spectra calculated with the CMP models with the same volume of ice and a pollution of 10 Vol-%: higher FIR values: $b/a = 1.62$ and $c = 45$ nm (ice/silicate = 3.25) lower FIR values: $b/a = 1.145$ and $c = 12$ nm (ice/silicate = 0.5)

– In the FIR and submm-region the spectrum is not affected by changes in the density distribution of the envelope, if the envelope mass is fixed. This part of the spectrum is also not affected by the scattering properties of the grains. The FIR and submm spectrum depends only on the mass of the envelope, when the luminosity and the radius are fixed and a certain dust model is chosen.

Therefore, the shell mass can be determined by fitting only the FIR and submm fluxes, when the distance and the luminosity of the source together with the radius of the envelope are known.

3.1. Spectra of a model protostellar envelope

Now we want to look at the differences in the spectra calculated with the different dust models. We first consider a particular model of an embedded protostar and then compare the results of radiative transfer calculations using different dust models.

We assume a protostar with a luminosity of 5 $L_\odot$ and an effective temperature of 4800 K. This protostar is embedded in a dusty envelope with a density distribution given by $\rho \propto r^{-1}$ that extends to $10^{16.5}$ cm = 2122 AU. The inner boundary radius of the dust shell is equal to the sublimation radius of the aC grains at $\approx 10^{12.2}$ cm. To calculate the values of the flux density, a distance of the source of 150 pc is assumed, typical for the nearest molecular clouds.

Now there are two ways to compare spectra with different dust models: The first is to fix the total mass (dust & gas) of the envelope and only change the properties of the grains. Here the value of 0.025 $M_\odot$ for the mass of the envelope is used. The disadvantage of this method is, that different dust models lead to different optical depths of the envelope. To seperate this effect from the change of the relative opacity (normalized at 200 μm) a second method is applied. The mass of the envelope is chosen so that the total optical depth of the envelope is fixed at the value $\tau_{200} = 0.01$. In the following, both methods are applied to all dust models.

In Fig. 9 we show the spectra calculated with the models with different b/a and 10 Vol-% pollution. In the model with fixed envelope mass the dust masses behave according to the different accreted mantles like 1:1.4:2. This is exactly the ratio between the fluxes at the FIR wavelengths. The normalization for a fixed τ_{200} value is, therefore, the same as for a constant dust mass.

The spectrum is found to be very sensitive to the coating thickness. With increasing coating thickness the spectral energy distribution is gradually shifted from NIR wavelengths to FIR. The comparison of spectra with constant optical depth exhibits considerable differences from the NIR up to the FIR.

The effects for the spectra of the different models with constant mantle thickness are very similar and are thus not shown.

© European Southern Observatory • Provided by the NASA Astrophysics Data System

1993A&A...279..577P

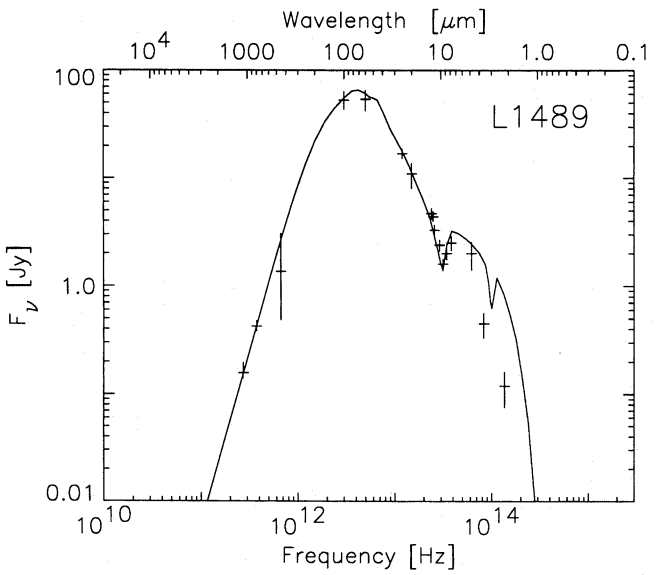

Fig. 12. Fit of the IR source in L1489

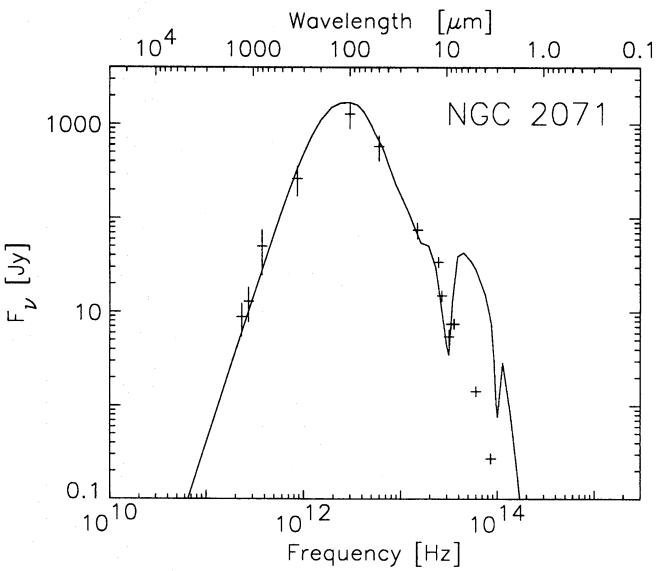

Fig. 13. Fit of the IR source in NGC 2071

In Fig. 10 spectra with b/a = 1.62 and varying degrees of pollution are shown. Whereas in the last picture the differences in the spectra partly result form the increasing mass of dust with increasing mantle thickness, here the total dust mass is nearly equal in all three cases. This means that the distribution of the aC between the free aC grains and the pollution of the ice mantles has a significant influence on the spectra, because aC in the ice leads to a higher opacity than the same amount of aC as free grains.

In Fig. 11 we compare spectra of dust models with equal total volumes of ice, equal pollution but different distribution of the ice on the grains. It can be seen that there are no sigificant differences between the models with constant core-mantle ratio and those with constant mantle thickness.

We conclude that the distribution of a given amount of ice and aC pollution on the grains (whether constant or variable mantle thickness) has almost no influence on the spectra. However, the spectra depend strongly on the relative amount of aC in the ice and (of course) on the total mass of dust.

3.2. Fit calculations

Each of our dust models is now used to fit the observed spectra of two protostellar sources. The first source is IRAS 04015+2610, located in the dark cloud L1489. Myers et al. (1987) observed this source between 0.4 μm and 20 μm, Beichmann et al. (1986) supplied IRAS-data and Zinnecker et al. (1992) carried out submm observations.

From the NIR images of Heyer et al. (1990) and the distance of 140 pc given by Myers et al. (1987) we assume the outer radius of the envelope to be $10^{16.5}$ cm. The luminosity is chosen to be $L = 5\,L_\odot$ in accordance to the value determined by Zinnecker et al. (1992). The effective temperature of the central object was set to 4900 K.

In Fig. 12 a fit of this source with the dust model with b/a = 1.145 CMP and 10 Vol-% pollution is shown. For the fit we assumed a density distribution of the form

$$\varrho(r) \sim \begin{cases} r^{-0.7} & r < 10^{15.8}\ \text{cm} \\ r^{-1.5} & 10^{15.8}\ \text{cm} \le r < 10^{16.5}\ \text{cm} \\ 0 & r \ge 10^{16.5}\ \text{cm}\,. \end{cases} \quad (4)$$

The fit is not perfect, because it predicts too much NIR radiation. This can be fixed only by accepting worse agreement at MIR wavelengths. In particular, a better fit of the NIR region would lead to a deeper absorption feature around 10 μm. As mentioned above, the NIR part of the spectrum depends strongly on the details of the density distribution and the scattering properties of the grains. It would also be very sensitive to the possible existence of a disk and its orientation. The scattering of stellar light in an flattened structure would be able to explain the deviations (see also Gürtler et al. 1991). We thus decided to fit the longer wavelengths at the costs of a poor NIR fit. The mass determined from the fits is not affected by these considerations. The resulting total mass of the envelope is $M = 0.071 M_\odot$.

The fits of the same source with the other dust models (not shown) were all performed with the same luminosity and outer radius of the envelope, to be consistent. We had to change the density distribution only slightly and obtained of course other masses. The problem with the high NIR fluxes is qualitatively the same for all dust models. The values for the masses obtained with the different dust models are shown in Table 2.

The second source is an IR source sited in NGC 2071. It is described in detail by Butner et al. (1990), from which the fluxes were also taken. We assume a luminosity $L = 520\,L_\odot$ and an effective temperature of the central object of 16 000 K as used by Butner and set the outer radius of the envelope to $10^{17.5}$ cm.

In Fig. 13 we present our fit of this source with the same dust model as above. Again we favour a good fit at MIR and

© European Southern Observatory • Provided by the NASA Astrophysics Data System

1993A&A...279..577P

Table 2. Fit masses in solar masses

	L 1489			NGC 2071		
CMP model	5 %	10 %	20 %	5 %	10 %	20 %
b/a= 1.145	0.076	0.071	0.054	60.4	51.4	44.8
b/a= 1.62	0.022	0.027	0.015	37.3	25.2	17.8
b/a= 2	0.028	0.019	—	21.9	13.8	—
c= 3 nm	0.083	0.081	0.078	63.3	59.1	52.7
c= 12 nm	0.066	0.062	0.053	51.6	48.0	43.9
c= 45 nm	0.045	0.032	0.016	31.7	25.2	10.7

longer wavelengths against the agreement in the NIR. We used a density distribution

$$\varrho(r) \sim \begin{cases} r^{-0.6} & r < 10^{15.6}\ \mathrm{cm} \\ r^{-0.1} & 10^{15.6}\ \mathrm{cm} \le r < 10^{17.5}\ \mathrm{cm} \\ 0 & r \ge 10^{17.5}\ \mathrm{cm} \end{cases} \quad (5)$$

and obtained a mass $M = 51.4\,M_{\odot}$. The masses obtained by fitting these source with the other dust models are also given in Table 2.

For both spectra, the dust model with $c = 3$ nm and 5 Vol-% pollution, i.e. the lowest ice and aC content in the CMP yields the highest fit masses, whereas the model with $c = 45$ nm and 20 Vol-% pollution yields the lowest ones. That can be expected from a look at the opacities of the models, because high opacity values yield low masses and vice versa. The factor between the maximum and the minimum mass is 5.1 for the spectrum of L1489 and 5.9 for NGC2071.

Since one never knows the actual mantle thicknesses and pollution concentrations in the CMP in protostellar envelopes, we conclude that the error made determing the mass through fit calculations, due to the unknown properties of the CMP, is up to a factor of 5.

4. Conclusions

We have shown, that ice mantles on dust grains in the envelopes of protostars can considerably influence the envelope opacity over a broad wavelength range.

Although the opacity is not sensitive to the structure of the mantles it is sensitive to the total amount of ice on the grains and it depends very strongly on the content of absorbing material in the ice coatings. Carbon grains embedded into the coatings absorb much more efficiently than free carbon grains. Due to the occurence of amorphous carbon in cold regions of the envelopes instead of graphite the power law index of the dust emissivity is always less than 2 and has a typical value between 1.4 and 1.5. Therefore, the opacities at long wavelengths are considerably higher than in models with graphite.

With the proposed dust models it is possible to fit the observed fluxes of protostellar sources in the FIR and MIR very well. The low quality of the fits in the NIR is probably due to uncertainties in the density distribution and the geometry of the sources. The determined envelope masses depend on the assumed ice mantle thickness and pollution and are therefore uncertain by a factor of 5.

Acknowledgements. We want to thank H. Mabilat, who helped perform the fit calculations and E. Thamm for his support in calculating the refractive indices. This project was supported by the DFG under grants He 1935/1-1,2 and Yo 5/7-2

References

Beichman, C.A., Myers, P.C., Emerson, J.P. et al., 1986, ApJ, 307, 337
Blanco A., Fonti, S.& Rizzo, F., 1991, Infrared Phys., 31, 167
Bohren, C.F. & Huffman, D.R., 1983, Absorption and scattering of light by small particles, John Wiley, New York
Boss, A.P., 1987, in: Interstellar Processes, eds. D.J. Hollenbach, H.A. Thronson, D. Reidel, Dordrecht, p. 321
Bussoletti, E., Colangeli, L., Borghesi, A.& Orofino, V., 1987, A&AS, 70, 257
Bussoletti, E., Fusco, C.& Longo, G. (Eds.), 1988, Experiments on Cosmic Dust Analogues, Kluwer Acad. Publ., Dordrecht
Butner, H. M., Evans II, N.J., Harvey, P.M. et al., 1990, ApJ, 364, 164
Butner, H. M., Evans II, N.J., Lester, D.F., Levreault, R.M. & Strom, S.E., 1991, ApJ, 376, 636
Chen, W.P. & Graham, J.A., 1993, ApJ, 409, 319
Czyzak, S.J. & Santiago, J.J., 1973, Ap&SS, 23, 443
Draine, B.T, 1985a, in: Protostars and planets II, eds. Black, D.C. & Matthews, M.S., University of Arizona Press, Tucson, p. 621
Draine, B.T, 1985b, ApJS, 57, 587
Draine, B.T & Lee, H.M., 1984, ApJ, 285, 89
Edoh, O., 1983, Ph.D. thesis, Univ. of Arizona
Emerson, J.P., 1988, in: Formation and Evolution of Low Mass Stars, eds. A. K. Dupree, M. T. V. T. Lago, Kluwer, Dordrecht, p. 21
Gürtler, J., Henning, Th., Krügel, E. & Chini, R., 1991, A&A, 252, 801
Hagen, W., Tielens, A.G.G.M., Greenberg, J.M., 1983 A&A, 117, 132
Heyer, M.H., Ladd, E.F., Myers, P.C. & Campbell, B.G., 1990, AJ, 99, 1585
Hyland, A.R. & Robinson, G., 1991, Proc. Astron. Soc. Aust., 9, 124
Kittel, C., 1963, Introduction to Solid State Physics, Wiley, New York
Lang, K.R., 1974, Astrophysical Formulae, Springer, Berlin
Lee, H.M. & Draine, B.T., 1985, ApJ, 290, 211
Leger, A., Gauthier, S., Defourneau, D. & Rouan, D., 1983, A&A, 117, 164
Leung, C.M., 1975, A&A, 199, 340
Martin, P.G. & Rogers, C., 1987, ApJ, 322, 374
Mathis, J.S., Rumpl, W. & Nordsieck, K.H., 1977, ApJ, 217, 425
Morton, D.C., 1974, ApJ, 193, L35
Mukai, T. & Krätschmer, W., 1986, Earth, Moon and Planets, 36, 145
Myers, P.C., Fuller, G.A., Mathieu, R.D. et al., 1987, ApJ, 319, 340
Ossenkopf, V., 1991, A&A, 251, 210
Ossenkopf, V., 1993, A&A, submitted

© European Southern Observatory • Provided by the NASA Astrophysics Data System

1993A&A...279..577P

Ossenkopf, V., Henning, Th. & Mathis, J.S., 1992, A&A, 261, 567
Pendleton, Y., Tielens, A.G.G.M. & Werner, M.W., 1988, BAAS, 20, 958
Pollack, J.B., McKay, C. & Christofferson, B., 1985, Icarus, 64, 471
Preibisch, Th., 1992, Diplom thesis, Julius-Maximilians-Universität Würzburg
Rouleau, F. & Martin, P.G., 1991, ApJ, 377, 526
Seki, J. & Hasegawa, H., 1983, Ap&SS, 94, 177
Shu, F.H., Adams, F.C. & Linzano, S., 1987 ARA&A, 25, 23
Sorrell, W.H., 1990a, MNRAS, 243, 570
Sorrell, W.H., 1990b, Wisc. Astrophys., 378
Tielens, A.G.G.M., 1989, in: Interstellar Dust, IAU Symp. 135, eds. L.J. Allamandola & A.G.G.M. Tielens, Kluwer, Dordrecht, p. 239
Tielens, A.G.G.M. & Hagen, W., 1982, A&A, 114, 245
Yorke, H.W., 1980a, A&A, 85, 215
Yorke, H.W., 1980b, A&A, 86, 286
Yorke, H.W., 1985, in: Birth and Infancy of Stars, eds. R. Lucas, A. Omont & R. Stora, Elsevier Science Publishers, p. 645
Yorke, H.W. & Shustov, B.M., 1981, A&A, 98, 125
Yorke, H.W., Bodenheimer, P., Laughlin, G., 1993, ApJ, 411, 274
Zinnecker, H., Bastien, P., Arcoragi, J.-P., & Yorke, H.W., 1992, A&A, 265, 726

This article was processed by the author using Springer-Verlag LaTeX A&A style file version 3.

© European Southern Observatory • Provided by the NASA Astrophysics Data System